Managing Energy Storage in Microgrids: A Multistage Stochastic Programming Approach

Arnab Bhattacharya, Jeffrey P. Kharoufeh, Bo Zeng, *Member, IEEE*

***Abstract*—A microgrid is a small-scale version of a centralized power grid that generates, distributes and regulates electricity flow to local entities using distributed generation and the main grid. Distributed energy storage systems can be used to mitigate adverse effects of intermittent renewable sources in a microgrid in which operators dynamically adjust electricity procurement and storage decisions in response to randomly-evolving demand, renewable supply and pricing information. We formulate a multistage stochastic programming (SP) model whose objective is to minimize the expected total energy costs incurred within a microgrid over a finite planning horizon. The model prescribes the amount of energy to procure, store and discharge in each decision stage of the horizon. However, for even a moderate number of stages, the model is computationally intractable; therefore, we customize the stochastic dual dynamic programming (SDDP) algorithm to obtain high-quality approximate solutions. Computation times and optimization gaps are significantly reduced by implementing a dynamic cut selection procedure and a lower bound improvement scheme within the SDDP framework. An extensive computational study reveals significant cost savings as compared to myopic and non-storage policies, as well as policies obtained using a two-stage SP model. The study also demonstrates the scalability of our solution procedure.**

***Index Terms*—Microgrid, energy storage, stochastic programming, stochastic dual dynamic programming.**

I. Introduction

ONE way of achieving deeper penetration of renewable energy sources into the electric power grid is the use of *microgrids*, which offer an incremental approach to deploying small-scale renewable sources, like wind and solar, in close proximity to local demand. Developed for a residential community, university, military-base, or other demand-side entities, a microgrid is a small-scale version of a centralized power grid that generates, distributes, and regulates electricity flow using local renewable generation sources [1], [2]. However, a deeper penetration of renewable sources in the overall energy portfolio poses a new set of challenges. Renewable sources are highly intermittent and uncertain in nature, making future supplies difficult to predict. Moreover, the limited generating capacity of renewable sources in microgrids makes them susceptible to real-time power shortages and reliability issues. Distributed energy storage systems, such as batteries or flywheels, serve to hedge against renewable uncertainty, and can be used to shift local energy consumption from peak-demand to low-demand periods [3], [4]. Moreover, with the advent of bidirectional technologies, operators in a microgrid can exploit dynamic pricing mechanisms by storing energy during off-peak periods for use in peak-price periods [5], [6]. With the growing appeal of renewable generation, dynamic strategies for procuring electricity and charging energy to, or discharging energy from, storage can be devised for microgrid entities to minimize their expected total costs in the presence of uncertain renewable sources, random demand, and time-varying electricity prices.

Correspondence to: Jeffrey P. Kharoufeh, Department of Industrial Engineering, University of Pittsburgh. Email:jkharouf@pitt.edu; Ph: +1-412-624-9832.

The literature related to optimal demand-side energy storage strategies is relatively small but is developing rapidly. Most prevalent are models that devise optimal demand-response schemes for consumers with elastic loads [7], [8]. However, such schemes have exhibited only a minor shift in consumer demand to match prices [9]. More recently, residential storage has emerged as a key facilitator of demand response on the consumer side [10], [11]. Earlier formulations of the demand-side storage management problem have employed a linear programming approach to minimize finite-horizon electricity costs assuming *a priori* knowledge of prices [12], [13]. Van de Ven et al. [14] examined a demand response problem under real-time pricing uncertainty using a finite-horizon Markov decision process (MDP) model. Proved was the existence of a dual-threshold, cost-minimizing optimal storage policy for a residential consumer with finite energy storage capacity. Hill et al. [15] developed simple threshold policies for grid-scale energy storage to mitigate negative impacts of solar energy integration while improving the overall real-time frequency response and voltage control capabilities of the grid. Koutsopoulos et al. [16] analyzed an optimal storage control problem under price and supply uncertainty. Using an infinite-horizon MDP model, they derived an optimal threshold policy for the online problem and proved its asymptotic optimality (as the storage capacity approaches infinity). However, none of these MDP models account for simultaneous uncertainty in demand, supply, and pricing, and they use relatively few scenarios to keep the problem dimension low. Furthermore, they are single-consumer models that do not consider network constraints and interactions between different microgrid entities.

Consequently, stochastic programming (SP) has emerged as a viable alternative to MDP models for problems with continuous actions and high-dimensional state spaces (cf. [17] for additional details). Lee et al. [18] formulated a two-stage linear SP model to minimize investment and ancillary-generation costs in a power network with high penetration of renewable sources and energy storage. They employed the well-known L-shaped algorithm [17] to solve the model in a day-ahead setting; however, a relatively small number of scenarios ($\approx$ 100) were considered. Ji et al. [19] proposed a two-stage stochastic, mixed-integer, quadratic programming

(SMIQP) model to jointly optimize the day-ahead operations of renewable sources and storage systems in a microgrid, also using a small number of scenarios. Xi et al. [20] addressed the problem of co-optimizing the real-time scheduling of storage usage for multiple applications, such as energy arbitrage and regulation services, while accounting for price and renewable uncertainty. They proposed a two-stage, stochastic mixed-integer programming (SMIP) model to obtain piecewise-linear value function approximations for a MDP model with continuous states and actions. Other representative two-stage SP models for similar problems can be found in references [21]–[24]. Generally speaking, most realistic SP models are NP-hard; however, their prevalence in the energy literature stems from the fact that several decomposition algorithms are available to solve such models efficiently [25]. By comparison, the literature is relatively sparse for multistage SP models that allow for recourse decisions at multiple stages of decision making. A key feature of multistage models is that they yield solutions that are *non-anticipative*, i.e., decisions made in any stage depend only on the information available up to that stage. By contrast, decisions from two-stage models are anticipative and may result in suboptimal strategies. However, multistage SP models are significantly harder to solve, and are intractable for even a moderate number of stages [26].

The main contributions of our work here can be summarized as follows. First, we propose a novel, multistage SP model to obtain viable procurement and storage operation strategies in a grid-connected microgrid. In this model, the initial (or first-stage) decisions are the storage capacities of local energy storage systems (e.g., batteries), subject to a budget constraint. During each subsequent stage of the planning horizon, multiple recourse decisions are made, including the total active and reactive power procured from the grid, the active power charged to, or discharged from, local storage systems, and the active and reactive power flowing in the lines based on a rigorous power flow model. The objective is to minimize the expected total energy costs incurred within the microgrid over a finite planning horizon, subject to storage capacity, line capacity, and other physical constraints. The model is distinguished from existing two-stage SP models in that non-anticipative procurement and storage decisions must be made in the face of multiple sources of uncertainty: demand, renewable supply and prices are all modeled as random variables. Second, to overcome the computational challenges associated with multistage SP models, we customize the stochastic dual dynamic programming (SDDP) algorithm [27] to obtain high-quality solutions for a 24-hour planning horizon. The algorithm is enhanced by implementing a dynamic cut selection (DCS) heuristic [28] to significantly reduce the SDDP computation time. Moreover, the SDDP algorithm is remarkably improved by employing a novel, yet pragmatic, lower bound enhancement procedure using Jensen's inequality. This refinement drastically reduces computation time and significantly improves solution quality, and it facilitates the use of a large number of potential scenarios. Our computational study demonstrates that very tight solution bounds are attainable within a reasonable amount of time. The results also suggest the scalability of our customized SDDP algorithm to problems of larger scale. Finally, the computational results reveal significant economic advantages as compared to myopic and non-storage policies, as well as policies obtained using a two-stage SP model.

II. Model Description

This section describes the multistage SP formulation to prescribe viable energy procurement and storage strategies for microgrid entities over a finite planning horizon. As in [29]–[31], we consider a grid-connected microgrid with a radial topology – a tree-like network of interconnected buses and power lines emanating from a reference bus (the *feeder*), which is connected to the main grid. The feeder is often connected to a distribution substation and delivers power procured from the main grid to other microgrid buses. Some or all of those buses have access to distributed storage systems. The operators use both distributed generation (e.g., wind and/or solar) and electricity procured from the main grid to satisfy the net demand and power flow constraints in each stage of the planning horizon. Surplus energy can be stored in finite-capacity storage systems for future use. The decision makers, who make procurement and storage decisions at the start of each stage, have access to real-time pricing information from an electricity spot market. However, the amount of energy that can be stored or made available for current or future stages is constrained by the capacity of the storage systems and power lines. Moreover, these decisions are subject to demand, renewable supply, and pricing uncertainty. The objective is to minimize the expected total energy costs incurred within the microgrid over the finite planning horizon.

A. Preliminaries

Consider a planning horizon of length Υ, and partition the time interval $[0, \Upsilon)$ so that

$$[0, \Upsilon) = \bigcup_{t=1}^{N} [\varepsilon_{t-1}, \varepsilon_t),$$

where N is the number of time intervals (or stages) and ε_t is the tth decision epoch with $\varepsilon_0 \equiv 0$ and $\varepsilon_N \equiv \Upsilon$. Therefore, the discrete time horizon is denoted by $T = \{1, \ldots, N\}$, where $t \in T$ is the index of the tth stage, namely $[\varepsilon_{t-1}, \varepsilon_t)$. Let $\delta_t \equiv (\varepsilon_t - \varepsilon_{t-1})$ denote the duration of the tth stage. Let $C = \{0, 1, \ldots, K\}$ be the finite set of buses in the microgrid, where bus 0 denotes the feeder connected to the main grid, and bus $i \in C \setminus \{0\}$ denotes the ith microgrid bus. It is assumed that the feeder is not connected to any load, renewable generator or storage device, and has a fixed voltage level. For notational convenience, we also define $T' \equiv T \setminus \{1\}$ and $C' \equiv C \setminus \{0\}$. The set of all lines in the microgrid is denoted by $A = \{(i, k) : i, k \in C\}$, where $(i, k) \in A$ is a power line connecting bus i to bus k.

Next, we describe the physical parameters of the microgrid. Let α be the maximum storage capacity of the microgrid, and $\beta_a(i, k)$ and $\beta_r(i, k)$ be the active and reactive power capacities (also known as nameplate capacities) of line (i, k). Let $\varphi(i, k)$ denote the impedance of line (i, k) such that

$$\varphi(i, k) = \lambda(i, k) + j\vartheta(i, k), \quad (i, k) \in A,$$

where $\lambda(i,k)$ and $\vartheta(i,k)$ denote the resistance and reactance of line (i,k), respectively, and $j=\sqrt{-1}$ is the unit imaginary number. Let ν denote the average per-unit cost of power lost due to resistive heating in any line $(i,k)\in A$. The quantity η_i denotes the average cost per unit energy charged to, or discharged from, the battery at bus i, while κ_i is the per-unit cost of battery capacity at bus i. The parameters ρ_c^i and ρ_d^i represent the charging and discharging efficiencies of the battery at bus i, respectively. The round-trip efficiency of the battery at bus i is defined as $\rho_i \equiv \rho_c^i\rho_d^i$ – a value that usually lies in the interval $[0.7, 0.9]$. The quantities τ_c^i and τ_d^i denote the maximum charging and discharging rates of the battery at bus i, respectively. Let $\gamma_{\min}^i$ and $\gamma_{\max}^i$ be the minimum and maximum proportions of battery capacity that can store energy, where $\gamma_{\min}^i, \gamma_{\max}^i \in (0,1)$. It is assumed that the batteries cannot self-discharge, i.e., energy is not dissipated when the batteries are not in use.

Now we describe the uncertain variables that evolve over the decision stages in T'. All random variables are defined on a common and complete probability space $(\Omega, \mathscr{A}, \mathbb{P})$. Let d_t^i denote the net-demand (demand minus renewable supply) realized per unit-time at bus i at the start of stage t, such that

$$d_t^i = r_t^i + jw_t^i, \quad (i,t)\in C\times T',$$

where r_t^i and w_t^i denote the active and reactive power components of d_t^i, respectively. Collect the net demand realizations in the vector $d_t \equiv ((r_t^i, w_t^i) : i \in C')$. Let p_t denote the real-time price realized at the start of stage t. Then for each $t\in T'$, the bounded vector $\omega_t \equiv (d_t, p_t) \in \Omega_t$ denotes the stage t realization of the random vector $\widetilde{\omega}_t$. Assume $|\Omega_t|<\infty$ for all $t\in T'$. It is noted that $\Omega_t \subseteq \mathbb{R}^M$, where $M \le 2K-1$. Henceforth, we refer to a scenario $\omega\in\Omega\equiv\Omega_2\times\cdots\times\Omega_N$ as a realization (or sample path) of the stochastic process $\{\widetilde{\omega}_t : t\in T'\}$.

In the following subsection, we define the decision variables and constraints of the model, and formulate a multistage SP model using the DistFlow equations for radial networks.

B. Multistage Stochastic Optimization Model

Let x_1^i be the stage 1 battery capacity decision at bus i that incurs a cost $\kappa_i\, x_1^i$. The capacity decisions are made before any of the random variables are realized. Collect the stage 1 decisions in the vector $x_1 \equiv (x_1^i : i\in C')$. Let $c_1 \equiv (\kappa_i : i\in C')$ denote the cost vector in stage 1 so that the total cost in this stage is

$$c_1' x_1 = \sum_{i\in C'} \kappa_i\, x_1^i. \tag{1}$$

However, the capacity decisions are constrained by the maximum storage capacity of the microgrid as follows:

$$0 \le \sum_{i\in C'} x_1^i \le \alpha. \tag{2}$$

Unique to our model is the fact that, starting from stage 2 and moving forward in time, microgrid operators make recourse decisions at the start of each stage. The stage t recourse decisions, when ω_t is realized, are collected in the vector $x_t(\omega_t)$. Henceforth, for notational convenience, we suppress the dependence of x_t on ω_t and simply write x_t. For each $i\in C'$ and $(i,k)\in A$, the decision vector for stage $t\in T'$ is defined as $x_t \equiv (y_t^i, m_t^i, n_t^i, v_t^i, q_t(i,k), s_t(i,k), a_t, b_t)$, whose elements are as follows:

- y_t^i: energy storage level at bus i at the start of stage t;
- m_t^i: active power charged into the battery at bus i;
- n_t^i: active power discharged from the battery at bus i;
- v_t^i: voltage level at bus i
- $q_t(i,k)$: active power flow in line (i,k);
- $s_t(i,k)$: reactive power flow in line (i,k);
- a_t: active power procured from main grid at the feeder;
- b_t: reactive power procured from main grid at the feeder.

For each bus $i\in C'$, the battery levels in successive stages are coupled via

$$y_{t+1}^i = y_t^i + \delta_t(\rho_c^i m_t^i - n_t^i/\rho_d^i), \quad t\in T'. \tag{3}$$

An interpretation of (3) is that the energy stored in a battery equals the stored energy at the start of the current stage, minus (plus) the amount of energy discharged from (charged to) the battery in the current stage, scaled by the discharging (charging) efficiency parameter. Note that the power quantities m_t^i and n_t^i are multiplied by the factor δ_t to convert them into units of energy. It is assumed that the batteries are capable of charging or discharging active power only and not reactive power (cf. [31]–[33]). Because demand, renewable supply and prices exhibit diurnal seasonality [34], [35], storage operations are optimized over a planning horizon that covers at least one complete cycle of the seasonal variables. Therefore, the terminal storage levels of the batteries are set to their initial levels [36], [37]. Specifically, for all $i\in C'$,

$$y_1^i = y_N^i. \tag{4}$$

The power that is charged to, or discharged from, the storage device is constrained by the current storage level, as well as the charging and discharging rates of the battery. Therefore, for each $i\in C'$,

$$0 \le m_t^i \le \min\{\tau_c^i, \delta_t^{-1}(x_1^i - y_t^i)/\rho_c^i\}, \qquad t\in T', \tag{5}$$

$$0 \le n_t^i \le \min\{\tau_d^i, \delta_t^{-1}\,\rho_d^i y_t^i\}, \qquad t\in T'. \tag{6}$$

As battery life can be reduced due to excessive charging or discharging, for each $i\in C'$, battery levels in each stage are limited by the following state-of-charge (SOC) constraints:

$$\gamma_{\min}^i\, x_1^i \le y_t^i \le \gamma_{\max}^i\, x_1^i, \quad t\in T'. \tag{7}$$

Next, we describe constraints related to power flow in the lines. In contrast to transmission systems, where power flows are characterized using DC optimal power flow approximations, the DistFlow model is often adopted for distribution networks to calculate the complex power flow and voltage profiles. Several recent papers have justified using the DistFlow equations for microgrids [29], [31], [38]–[40]. Because power flow is directional, assume that $q_t(i,k)\ge 0$ when active power flows from bus i to bus k, and $q_t(i,k)<0$ if it flows from bus k to i; similar notation is adopted for the reactive component $s_t(i,k)$. For a given bus $i\in C'$, let Λ_i and Θ_i denote the parent bus and the adjoining children buses connected to bus i, respectively. The fixed voltage level at the feeder is denoted by

v_0. Then for each $i \in C'$ and $t \in T'$, the DistFlow equations are

$$q_t(\Lambda_i, i) = r_t^i + m_t^i - n_t^i + \sum_{k \in \Theta_i} q_t(i,k), \tag{8a}$$

$$s_t(\Lambda_i, i) = w_t^i + \sum_{k \in \Theta_i} s_t(i,k), \tag{8b}$$

$$v_t^i = v_t^{\Lambda_i} - \frac{\lambda(\Lambda_i, i) q_t(\Lambda_i, i) + \vartheta(\Lambda_i, i) s_t(\Lambda_i, i)}{v_0}. \tag{8c}$$

The left-hand side of (8a) represents the active power that flows into a bus from its parent, while the right-hand side is the net active power that flows out of the bus to its children, after accounting for the local active demand and battery power flows. Equation (8b) can be similarly interpreted for reactive power flows. Equation (8c) is used to compute the voltage level of bus i.

Power procured from the main grid is delivered to the microgrid via the feeder (bus 0). The DistFlow equations at the feeder are

$$a_t = \sum_{k \in \Theta_0} q_t(0,k), \qquad t \in T', \tag{9a}$$

$$b_t = \sum_{k \in \Theta_0} s_t(0,k), \qquad t \in T', \tag{9b}$$

where $a_t + jb_t$ is the net power injected into the microgrid via the feeder at stage t. To avoid reverse power flows at the feeder that can negatively affect operation of voltage regulators and protective devices [31], [41], we impose the following non-negativity constraint:

$$a_t \geq 0, \qquad t \in T'. \tag{10}$$

For any line $(i,k) \in A$, the active and reactive power flows are constrained by the nameplate capacities via

$$|q_t(i,k)| \leq \beta_a(i,k), \qquad t \in T', \tag{11}$$

$$|s_t(i,k)| \leq \beta_r(i,k), \qquad t \in T', \tag{12}$$

ensuring that power lines are not damaged due to resistive overheating [31], [42]. Additionally, distribution networks typically require the nominal voltage level at each bus to be maintained within a tolerance band [29], [30]. Therefore, the voltage level at each bus $i \in C'$ is constrained by the inequality

$$v_{\min}^i \leq v_t^i \leq v_{\max}^i, \quad t \in T', \tag{13}$$

where $v_{\min}^i$ and $v_{\max}^i$ denote the minimum and maximum voltage levels allowed at bus i, respectively.

It is noted that the decisions made at a current stage depend on the decisions made up to the previous stage via the temporal linking constraints (3). Thereby, the set of feasible decisions x_t in each stage $t \in T'$ is denoted by $\mathcal{X}_t(x_{t-1}, \omega_t)$, and this set is defined by the constraints (3) – (13) for each $(\omega, t) \in \Omega \times T'$.

Finally, we describe the objective function, which is to be minimized. Let c_t denote the cost vector in stage $t \in T'$ so that the total cost incurred in this stage is

$$c_t' x_t = p_t a_t \delta_t + \sum_{i \in C'} \eta_i (m_t^i + n_t^i) \delta_t + \sum_{(i,k) \in A} \nu \ell_t(i,k) \delta_t, \tag{14}$$

where $\ell_t(i,k)$ is the resistive power loss in line (i,k). The first term on the right-hand side of (14) is the total grid procurement cost, the second term is the total battery charge-discharge cost, and the third term represents the total cost incurred due to power-line losses in stage t. Each term on the right-hand side of (14) is multiplied by δ_t to convert power units to energy units. The battery cost rate η_i is assumed to be equal for both charging and discharging; however, this assumption can be relaxed. Using the DistFlow equations, the resistive power loss in line $(i,k) \in A$ can be closely represented by the quadratic function (see [33], [43])

$$\ell_t(i,k) = \lambda(i,k) \left(\frac{q_t(i,k)^2 + s_t(i,k)^2}{v_0^2} \right), \quad t \in T', \tag{15}$$

so the per-unit cost incurred due to power losses in line (i,k) at stage t is equal to $\nu \ell_t(i,k)$. Note that, because $\ell_t(i,k)$ is quadratic and convex, it can be readily approximated using piecewise-linear functions (cf. [44] in the context of the unit-commitment problem). This approach is commonly implemented by commercial optimization solvers (e.g., Gurobi) that exploit linear optimization algorithms to efficiently solve quadratic programs. Therefore, the multistage linear SP model can now be formulated and represented in the nested form

$$z = \min_{x_1} \; c_1' x_1 + \mathbb{E}_{\widetilde{\omega}_2} \left[\min_{x_2} c_2' x_2 + \mathbb{E}_{\widetilde{\omega}_3 | \widetilde{\omega}_2} \left[\min_{x_3} c_3' x_3 + \cdots + \mathbb{E}_{\widetilde{\omega}_N | \widetilde{\omega}_{N-1}} \left[\min_{x_N} c_N' x_N \right] \ldots \right] \right] \tag{16a}$$

$$\text{s.t.} \;\; x_t \in \mathcal{X}_t(x_{t-1}, \omega_t), \; \forall (\omega, t) \in \Omega \times T', \tag{16b}$$

$$0 \leq \sum_{i \in C'} x_1^i \leq \alpha, \tag{16c}$$

where $\mathbb{E}_{\widetilde{\omega}_i | \widetilde{\omega}_j}$ denotes the expectation taken with respect to the conditional probability measure $\mathbb{P}(\widetilde{\omega}_i | \widetilde{\omega}_j)$. Note that the nested structure of model (16) is a direct consequence of the multiple recourse opportunities available to the decision maker as information is progressively revealed over the planning horizon. This distinguishes model (16) from two-stage SP models that allow only a singular recourse opportunity under uncertainty [24], [45]. Unfortunately, model (16) is computationally intractable, even when the number of stages N is moderate (see [26], [27], [46] for additional details). However, in Section III, we describe how the stochastic dual dynamic programming (SDDP) algorithm can be used to obtain high-quality, approximate solutions to model (16).

III. Stochastic Dual Dynamic Programming (SDDP)

SDDP is a well-known decomposition procedure that can be used to solve multistage, stochastic programs with a large number of stages [27], [47]. The SDDP algorithm builds piecewise-linear outer approximations of the cost-to-go functions at each stage by randomly sampling from a finite set of scenarios. The algorithm iteratively updates the lower and upper bounds of the optimal value z of model (16) using a two-step procedure – a forward pass and a backward pass – and assumes stage-wise independence of the random variables.

The algorithm terminates once the bounds satisfy a prescribed convergence criterion.

To customize the SDDP algorithm, model (16) is first reformulated as an N-stage stochastic dynamic program. The first-stage (or stage 1) problem is defined as

$$z = \min_{x_1} \; c_1' x_1 + \mathbb{E}[Q_2(x_1, \widetilde{\omega}_2)] \qquad (17)$$
$$\text{s.t.} \;\; 0 \le \sum_{i \in C'} x_1^i \le \alpha,$$

where $Q_2(x_1, \omega_2)$ is the total future cost incurred under decision x_1 and realization $\omega_2 \in \Omega_2$. For $t \in T'$, the stage t problem is defined as

$$Q_t(x_{t-1}, \omega_t) = \min_{x_t} \; c_t' x_t + \mathbb{E}[Q_{t+1}(x_t, \widetilde{\omega}_{t+1})] \qquad (18)$$
$$\text{s.t.} \;\; F_t x_t = h_t(\omega_t) - G_t x_{t-1}.$$

In formulation (18), matrices F_t and G_t, and the vector $h_t(\omega_t)$, are obtained by reformulating constraints (3) – (13) as equality constraints. Let $\pi_t(\omega_t)$ denote the optimal dual vector associated with (18). In dynamic programming parlance, $Q_t(x_{t-1}, \omega_t)$ is the stage t cost-to-go (or value) function. Without loss of generality, assume $\mathbb{E}[Q_{N+1}(x_N, \widetilde{\omega}_{N+1})] = 0$ in the stage N problem; however, any continuous, convex function can be assumed for $\mathbb{E}[Q_{N+1}(x_N, \widetilde{\omega}_{N+1})]$.

To implement the SDDP algorithm, the scenarios of model (16) are stored as a finite scenario tree with N stages. A scenario tree originates at a *root* node that stores the first-stage decision x_1 and progressively branches to other child nodes that are defined by the number of possible stage t realizations $|\Omega_t|$ in stage $t \in T'$. The nodes in stage N are called the *leaf nodes*. The total number of leaf nodes equals the number of scenarios of (16). Figure 1 depicts a scenario tree with three stages and six scenarios. Because the number of scenarios, $|\Omega_2 \times \cdots \times \Omega_N|$, grows exponentially with N, problem (16) must be solved approximately to accommodate a planning horizon of 24 (or more) decision stages.

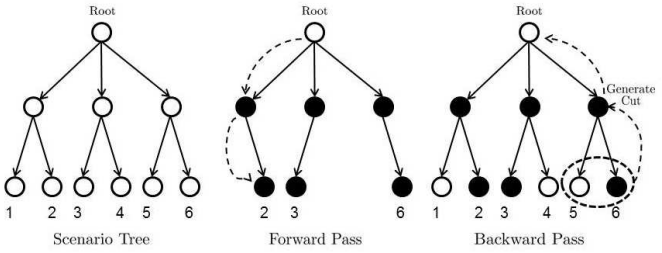

Fig. 1. Depiction of a scenario tree with three stages and six scenarios.

To solve (16) approximately, a finite number of scenarios are sampled from the scenario tree to develop a piecewise-linear outer approximation of $\mathbb{E}[Q_{t+1}(x_t, \widetilde{\omega}_{t+1})]$ in (18) for each stage t problem. The approximate stage t cost-to-go function is denoted by $\widehat{Q}_t(x_{t-1}, \omega_t)$. The outer approximations are developed by generating Bender's cuts

$$\theta_{t+1} \ge \bar{h}_{t+1,k} - \bar{\pi}_{t+1,k}' G_{t+1} x_t, \qquad k \in \mathcal{K}. \qquad (19)$$

In (19), the set $\mathcal{K}$ is the index set for all Bender's cuts added to each stage t problem (18). Here, column vector $\bar{\pi}_{t+1,k} \equiv \mathbb{E}[\pi_{t+1}(\widetilde{\omega}_{t+1})]$ defines the gradient and $\bar{h}_{t+1,k}$ is the intercept term for cut $k \in \mathcal{K}$, where

$$\bar{h}_{t+1,k} = \mathbb{E}[\widehat{Q}_{t+1}(x_t^k, \widetilde{\omega}_{t+1})] + \bar{\pi}_{t+1,k}' G_{t+1} x_t^k,$$

and x_t^k is a feasible stage t solution. Thus, the approximate stage t problem assumes the form

$$\widehat{Q}_t(x_{t-1}, \omega_t) = \min_{x_t} \; c_t' x_t + \theta_{t+1} \qquad (20)$$
$$\text{s.t.} \;\; F_t x_t = h_t(\omega_t) - G_t x_{t-1},$$
$$\theta_{t+1} \ge \bar{h}_{t+1,k} - \bar{\pi}_{t+1,k}' G_{t+1} x_t, \;\; k \in \mathcal{K}$$

while the approximate stage 1 problem is

$$\hat{z} = \min_{x_1} \; c_1' x_1 + \theta_2 \qquad (21)$$
$$\text{s.t.} \;\; \sum_{i \in C'} x_1^i \le \alpha,$$
$$\theta_2 \ge \bar{h}_{2,k} - \bar{\pi}_{2,k}' G_2 x_1, \;\; k \in \mathcal{K}$$
$$x_1 \ge 0.$$

Let $\hat{x}(\omega) \equiv (\hat{x}_t(\omega))_{t \in T}$ be an approximate policy obtained by solving problems (20) and (21) for scenario $\omega \in \Omega_2 \times \cdots \times \Omega_N$. In the forward pass of the SDDP algorithm, S distinct scenarios are sampled uniformly from the scenario tree using the well-known Monte-Carlo method (see [27], [28], [46]). Subsequently, the stage t problems are solved approximately for each of the sampled scenarios, starting from the first stage and moving forward to the final stage. At the completion of the forward pass, an upper bound to z is calculated, and a convergence criterion is tested. If the criterion is satisfied, the algorithm terminates; otherwise, the current optimal policy is amended by adding $|\Omega_t|$ Bender's cuts to each of the stage t problems associated with the sampled scenarios, starting from the last stage and working backwards to the first stage. Figure 1 depicts the forward and backward passes of the SDDP algorithm for a given scenario tree. Let $\Omega_S \subset \Omega$ be a finite set of S distinct scenarios ω sampled from Ω. The steps of the algorithm are summarized as follows:

1) **Sampling**
   Sample S distinct scenarios ω from Ω to form Ω_S.
2) **Forward Pass**
   2a) For $t = 1$, solve (21) and save $\hat{x}_1$ and $\hat{z}$;
   2b) For $t = 2, \ldots, N$ and $\omega \in \Omega_S$, solve (20) and store $\hat{x}_t(\omega)$ and $\widehat{Q}_t(\hat{x}_{t-1}(\omega), \omega_t)$, where ω_t is the $(t-1)$th component of ω.
3) **Convergence Test** (at the 95% confidence level)
   3a) Compute an upper bound of z by

$$z_u = c_1' \hat{x}_1 + (1/S) \sum_{\omega \in \Omega_S} \sum_{t=2}^{N} c_t' \hat{x}_t(\omega),$$

   and assign lower bound $z_\ell := \hat{z}$ by solving (21);
   3b) Terminate the algorithm if (see [27])

$$z_u + \left(1.96\, \hat{\sigma}_u / \sqrt{S}\right) - z_\ell \le \epsilon,$$

   where ϵ is a prescribed accuracy level, and $\hat{\sigma}_u$ is the sample standard deviation of the observations $\{z_\omega : \omega \in \Omega_S\}$ with

$$z_\omega = c_1'\hat{x}_1 + \sum_{t=2}^{N} c_t'\hat{x}_t(\omega);$$

Else go to Step 4.

4) **Backward Pass**

4a) For $t = 2, \ldots, N$ and $\omega \in \Omega_S$
- For each $\omega_t \in \Omega_t$, solve (20) using $\hat{x}_{t-1}(\omega)$, and save $\hat{\pi}_t(\omega_t)$ and $\widehat{Q}_t(\hat{x}_{t-1}(\omega), \omega_t)$;
- Generate a Bender's cut (19) and add it to all subproblems at stage $t-1$;

4b) Go to step 1.

IV. Improving the Performance of SDDP

The standard SDDP algorithm of Section III involves visiting S scenarios in the forward pass, and then a backward pass is performed to build $|\Omega_t|$ cuts for each stage t problem. This procedure yields an increasing number of Bender's cuts for each stage t problem, not all of which are active at each iteration of the algorithm. To reduce the computational burden of solving problems (20) and (21), a more sensible approach is to select cuts for the current iteration from a collection of cuts that have been generated in prior iterations. While there exist several classes of cut selection procedures in the stochastic programming literature (cf. [17], [46]), an effective dynamic cut selection (DCS) procedure due to de Matos et al. [28] was implemented to reduce the computation time of the standard SDDP algorithm.

A. Dynamic Cut Selection (DCS) Heuristic

In the DCS procedure, cuts are added iteratively rather than adding all cuts at once. At each iteration of the SDDP algorithm, a sequence of values $V_k \equiv (\bar{h}_{t+1,k} - \bar{\pi}'_{t+1,k} G_{t+1}\hat{x}_t)$ are computed for all $k \in \mathcal{K}$ (the index set of all cuts generated in prior iterations) and $\hat{x}_t$ is the current optimal solution at stage t. If the cut $k^* = \text{argmax}_k\{V_k\}$ has not been added to (20) yet, then k^* is added to (20) and re-solved. Moreover, at each stage $t \in T'$, the cuts that were generated for the stage t problems, associated with the scenarios visited in prior iterations, can be accessed to determine the set of active cuts for the stage t problems in the current iteration. Consequently, a broad set of cuts are retained that are likely to be important to all the subproblems at a given stage. Note that at the start of a new iteration, cuts of all the stage problems are cleared. However, the cuts are not discarded because one cannot ensure that a currently inactive cut will remain inactive for other scenarios visited at a later iteration. Thus, the algorithm has access to all the cuts generated in earlier iterations, and only adds the active cuts to the stage t problems during the forward and backward passes of the current iteration. The steps of the algorithm are summarized as follows:

1) **Remove cuts**
Remove the cuts from all stage t problems (20) and the stage 1 problem (21).
2) **Sampling**
Sample S distinct scenarios ω from Ω to form Ω_S.
3) **Forward Pass**

3a) For $t = 1$, solve (21) and save $\hat{x}_1$ and $\hat{z}$;

3b) For $t = 2, \ldots, N$ and $\omega \in \Omega_S$
- Solve (20) and store $\hat{x}_t(\omega)$ and $\widehat{Q}_t(\hat{x}_{t-1}(\omega), \omega_t)$, where ω_t is the $(t-1)$th component of ω;
- If $k^* = \text{argmax}_k\{\bar{h}_{t+1,k} - \bar{\pi}'_{t+1,k} G_{t+1}\hat{x}_t(\omega)\}$ is not in (20), then add cut k^* and re-solve (20).

4) **Convergence Test**
Identical to Step 3 of the standard SDDP algorithm.

5) **Backward Pass**

5a) For $t = 2, \ldots, N$ and $\omega \in \Omega_S$
- For each $\omega_t \in \Omega_t$, solve (20) using $\hat{x}_{t-1}(\omega)$, and save $\hat{\pi}_t(\omega_t)$ and $\widehat{Q}_t(\hat{x}_{t-1}(\omega), \omega_t)$;
- If $k^* = \text{argmax}_k\{\bar{h}_{t+1,k} - \bar{\pi}'_{t+1,k} G_{t+1}\hat{x}_t(\omega)\}$ is not in (20), then add cut k^* and re-solve (20);
- Generate a Bender's cut (19) and add it to all subproblems at stage $t-1$;

5b) Go to step 1.

B. Lower Bound Improvement via Jensen's Inequality

The DCS heuristic reduces the number of cuts that are added at each stage; however, it cannot guarantee the strength of these cuts. The standard SDDP algorithm exhibits slow convergence because the lower bounds obtained from the approximate stage t problems – which do not exploit strong valid inequalities – are relatively weak (cf. [48], [49]). To address this shortcoming, we propose a lower bound improvement scheme that makes use of Jensen's inequality (see [50], p. 188). The idea is to generate a set of strong valid inequalities during the backward pass of the SDDP algorithm. First, the elements of an artificial scenario, $\bar{\omega} \equiv (\bar{\omega}_2, \ldots, \bar{\omega}_N)$, are obtained by

$$\bar{\omega}_t = \sum_{\omega_t \in \Omega_t} \omega_t / |\Omega_t|, \quad t \in T'.$$

We call $\bar{\omega}$ the average scenario and note that it may not necessarily belong to Ω. Next, during a backward pass of the SDDP algorithm, a valid inequality of the form

$$\theta_{t+1} \geq Q_{t+1}(x_t, \bar{\omega}_{t+1}), \quad t \in T, \tag{22}$$

is added to each approximate stage t problem. The right-hand side of inequality (22) is evaluated by setting $x_t = \hat{x}_t$, where $\hat{x}_t$ is the current optimal solution at stage t. Because $\bar{\omega}$ is computed *a priori*, and $\hat{x}_t$ is known for each $t \in T'$ from the forward pass, adding cut (22) does not impose any additional computational burden. Note that, for a given feasible solution x_t, the inequality $\theta_{t+1} \geq \mathbb{E}[Q_{t+1}(x_t, \widetilde{\omega}_{t+1})]$ holds because problem (20) is a relaxation of problem (18). Furthermore, we have that $\mathbb{E}[Q_{t+1}(x_t, \widetilde{\omega}_{t+1})] \geq Q_{t+1}(x_t, \bar{\omega}_{t+1})$ by Jensen's inequality. Therefore, the cuts (22) are valid inequalities for the approximate stage t problems. The computational results of Section V reveal that the addition of these valid inequalities significantly improves solution quality and drastically reduces computation time, as compared to the standard SDDP algorithm.

V. Computational Results

This section presents computational results illustrating procurement and storage policies obtained by solving problem (16) approximately using standard SDDP, its DCS variant (SDDP+DCS), and the lower bound improvement scheme integrated within SDDP+DCS (SDDP+DCS+J), as described in Sections III, IV-A and IV-B, respectively. First, detailed descriptions of the source data, microgrid configuration and computational study are provided.

A. Data Description

Hourly demand and real-time electricity pricing data were obtained from PJM Interconnection (http://pjm.com/), while hourly wind speed data were obtained from the National Renewable Energy Laboratory (http://nrel.gov/) for the years 2012 and 2013. Wind speeds were converted to active wind-power outputs for a small-scale wind turbine by applying equation (13) of [51]. Moreover, reactive wind-power outputs were obtained from the PQ characteristic curve of a small wind turbine; for more details, see [52]. As price and wind levels are highly seasonal, the original data were partitioned into two disjoint sets, each spanning one year. As an aid to data visualization, for each data set, 95% confidence intervals (c.i.) were constructed for hourly demand, wind-generation and price levels by fitting truncated normal distributions whose parameters were estimated via maximum likelihood estimation (MLE). Figure 2 depicts the average electricity prices and wind-generation levels over a 24-hour period for the year 2012. Note that midnight is 0000 so that hour 1 corresponds to 0000 to 0100, hour 2 is 0100 to 0200, and so forth.

B. Microgrid Configuration

We consider a 4-bus microgrid configuration as depicted in Figure 3. The 4-bus system is powered by the main grid and a small-scale wind turbine that is connected to a single local storage device located at bus 3, which implies that $x_1^i = 0$ for all $i \in C' \setminus \{3\}$. In what follows, let $\bar{r}_t^i$ and $\bar{w}_t^i$ denote the sample means of the active power ($\tilde{r}_t^i$) and reactive power ($\tilde{w}_t^i$) components of net demand, respectively, in stage $t \in T'$ at bus $i \in C'$. Denote the associated sample variances by $\hat{r}_t^i$ and $\hat{w}_t^i$, respectively. The net demand components at bus $i \in C'$ are assumed to follow truncated normal distributions, i.e.,

$$\tilde{r}_t^i \sim TN(\bar{r}_t^i, \hat{r}_t^i), \quad t \in T', \tag{23}$$

$$\tilde{w}_t^i \sim TN(\bar{w}_t^i, \hat{w}_t^i), \quad t \in T'. \tag{24}$$

For each stage t, the (finite) supports of the random variables $\tilde{r}_t^i$ and $\tilde{w}_t^i$ were determined using the maximum and minimum levels of net demand obtained from the PJM demand and NREL wind data.

The loads connected to buses 1 and 2 are assumed to be homogenous with identical active power distributions, i.e.,

$$\tilde{r}_t^1 \overset{d}{=} \tilde{r}_t^2, \quad t \in T'.$$

Moreover, both loads are assumed to have high power factors (the ratio of active to apparent power) and, therefore, consume negligible reactive power. Thus,

$$\tilde{w}_t^1 = 0 \quad \text{and} \quad \tilde{w}_t^2 = 0, \quad t \in T'.$$

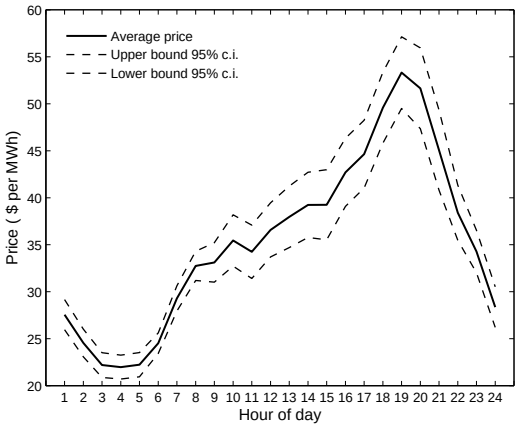

(a) Real-time hourly electricity prices.

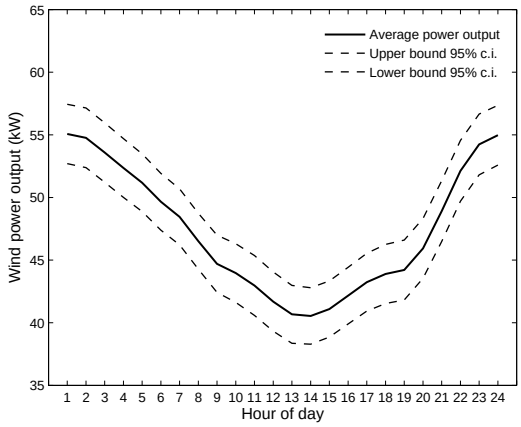

(b) Hourly wind-generation levels.

Fig. 2. Average price and wind-generation levels for the year 2012.

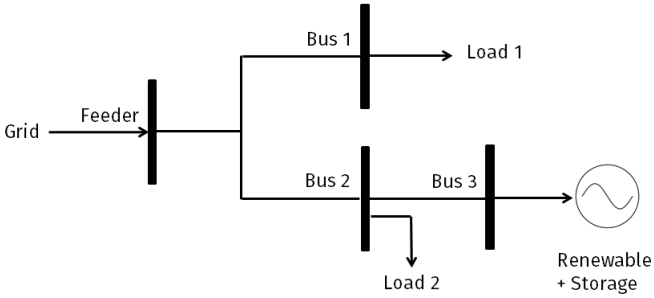

Fig. 3. A 4-bus, grid-connected microgrid.

The wind turbine connected to bus 3, on the other hand, generates both active and reactive power in each stage t.

The microgrid operators are assumed to be price-takers with no demand-response capabilities. However, simple demand-response schemes can be integrated into the model without imposing additional computational burden. Microgrid operators have access to the main grid at all times and can procure electricity at spot prices that also follow truncated normal distributions of the form

$$\tilde{p}_t \sim TN(\bar{p}_t, \hat{p}_t), \quad t \in T', \tag{25}$$

where $\bar{p}_t$ and $\hat{p}_t$ are the sample mean and variance of the price at stage t, respectively.

The power lines are all assumed to have identical line capacities (β_a, β_r), resistance (λ) and reactance (ϑ) values. A deep-cycle, lead-acid battery with a shelf-life of over 24 hours is used as the storage device at bus 3. The battery parameters $(\kappa, \eta, \rho_c, \rho_d, \tau_c, \tau_d, \gamma_{\min}, \gamma_{\max})$ are selected based on information provided in [53]. It is assumed that the battery is charged up to its maximum SOC level at the start of the planning horizon, i.e., $y_1 = \gamma_{\max} x_1$, and therefore, the terminal battery level is $y_N = y_1 = \gamma_{\max} x_1$ by (4). The voltage limits $(v_{\min}, v_{\max})$ at each bus were set to $\pm 5\%$ of the feeder voltage v_0 (see [30], [31]). Table I summarizes the parameter values used in the computational experiments.

TABLE I
PARAMETER VALUES FOR THE PROBLEM INSTANCES.

Parameter	Parameter description	Value
α	Maximum battery capacity (kWh)	60.00
κ	Per-unit cost of battery capacity ($/kWh)	50.00
η	Per-unit cost of charging/discharging ($/kWh)	2.00
τ_c	Charging rate of the battery (kW)	25.00
τ_d	Discharging rate of the battery (kW)	25.00
ρ_c	Charging efficiency of the battery	0.95
ρ_d	Discharging efficiency of the battery	0.90
$\gamma_{\min}$	Minimum battery SOC fraction	0.10
$\gamma_{\max}$	Maximum battery SOC fraction	0.90
β_a	Line capacity for active power (kW)	60.00
β_r	Line capacity for reactive power (kVAR)	60.00
λ	Line resistance (Ohm)	0.009
ϑ	Line reactance (Ohm)	0.009
v_0	Fixed voltage level at the feeder (kV)	10.00
$v_{\min}$	Minimum bus voltage level (kV)	9.50
$v_{\max}$	Maximum bus voltage level (kV)	10.50

C. Description of Experiments

For the computational experiments, a 24-hour planning horizon in the year 2012 was considered, i.e., $T = \{1, \ldots, 25\}$, where hour 1 is stage 2, hour 2 is stage 3 and so forth; hence, $\delta_t = 1$ for each t. The standard SDDP, SDDP+DCS and SDDP+DCS+J algorithms were coded in Python 2.7 and solved using the Gurobi 6.5 solver. The piecewise-linear approximation to (15) was created using the default settings of Gurobi, and the dual-simplex method was selected as the default linear programming (LP) solver. The algorithms were implemented on a 64-bit, 4th generation Intel® Core™ i7, 64 GB, 2.9 GHz Windows machine.

We considered different combinations of the number of sampled scenarios (S) in the forward pass, and the number of stage t realizations $(|\Omega_t|)$ for the backward pass, holding $|\Omega_t|$ constant for all $t \in T'$. The parameter S was varied from 50 to 250 in increments of 50, while $|\Omega_t|$ was varied from 5 to 20 in increments of 5. For each $t \in T'$, a set of $|\Omega_t|$ samples were first generated to construct a scenario tree before running any of the three procedures. To generate the samples $\omega_t \equiv (r_t^i, w_t^i, p_t : i \in C')$ at each stage t, a multivariate truncated normal distribution was used in which each marginal distribution is also truncated normal. The sampling procedure was further simplified by assuming that the random variables at each stage are all mutually independent, i.e., for each $t \in T'$

$$\mathcal{F}_t(\omega_t) = \mathcal{P}_t(p_t) \prod_{i=1}^{3} \mathcal{R}_t^i(r_t^i) \mathcal{W}_t^i(w_t^i), \quad \forall \omega_t \in \Omega_t,$$

where $\mathcal{F}_t$ is the joint probability density function (p.d.f.), and $\mathcal{P}_t$, $\mathcal{R}_t^i$, and $\mathcal{W}_t^i$ are the stage t marginal p.d.f.s of price (25), active power (23) and reactive power (24) components of net demand at bus i, respectively. Alternative sampling procedures can be used, such as those described in [54]; however, we chose this sampling procedure to satisfy the stage-wise independence criterion of the SDDP algorithm. For comparison purposes, the same $|\Omega_t|$ samples were used to generate scenario trees for all three procedures.

Once a scenario tree is generated, S distinct forward-pass scenarios $\omega \equiv (\omega_t : t \in T')$ are uniformly sampled from the scenario tree in each iteration of the three procedures. It is worth noting that empirical forecast distributions, based on forward bootstrapping techniques [55], can also be used to sample scenarios; however, our main purpose here is to illustrate the usefulness of the SP model and its solutions. The quality of solutions obtained using standard SDDP, SDDP+DCS, and SDDP +DCS+J algorithms was assessed by computing the approximate gap percentage

$$\text{Gap } (\%) = \frac{z_u - z_\ell}{z_\ell} \times 100. \tag{26}$$

All three procedures were terminated if either the SDDP convergence criterion was satisfied (with $\epsilon = 10^{-5}$), or 500 iterations were completed, whichever occurred first.

D. Results and Discussion

The computational results for the standard SDDP procedure are provided in Table II. It is noted that for a fixed number of scenarios S, the gap percentage decreases sharply as $|\Omega_t|$ increases; however, as one might expect, the computation times increase. Specifically, if additional state information is used at each stage to develop Bender's cuts, better value-function approximations are obtained; however, a far greater number of stage t problems must be solved. Similarly, for a fixed value of $|\Omega_t|$, the gap percentages decrease, and the computation time increases (but only moderately) as S increases. This trend stems from the fact that the lower bounds progressively improve, albeit slowly, as more scenarios are sampled, but a larger number of stage t problems must be solved in each iteration. However, the reported gap percentages indicate that the bounds are not tight. For example, when $S = 250$ and $|\Omega_t| = 20$, solving the model for over 6.7 hours reduced the gap to only 6.96%.

Table III summarizes the results when using the standard SDDP algorithm supplemented with DCS. The table reveals that both solution quality and computation time improved, relative to the results for standard SDDP. For instance, when $S = 250$ and $|\Omega_t| = 20$, SDDP+DCS reduces the gap percentage by a factor of over 2.3 (from 6.96% to 3%). Additionally, the computation time is reduced by a factor of nearly 1.3 (from 403.64 min to 311.37 min). However, the gap percentages for SDDP+DCS are still high in absolute terms, which points to a slow rate of convergence of the lower bounds z_ℓ. In fact, for both the SDDP and SDDP+DCS procedures, the lower bounds converged rapidly in the first few iterations, and converged very slowly thereafter. For example, when $S = 250$ and $|\Omega_t| = 20$, the SDDP +DCS lower bound

TABLE II
RESULTS USING THE STANDARD SDDP ALGORITHM.

S	$\lvert\Omega_t\rvert$	z_ℓ	z_u	Gap %	Time (mins)
50	5	62.46	78.03	24.93	48.76
	10	66.28	77.64	17.14	64.85
	15	68.89	77.21	12.08	98.33
	20	69.8	77.02	10.34	132.65
100	5	63.42	77.97	22.94	61.28
	10	67.24	77.28	14.93	92.37
	15	69.72	77.15	10.66	131.54
	20	70.23	77.01	9.65	189.95
150	5	64.45	77.56	20.34	73.89
	10	67.93	77.15	13.57	129.76
	15	69.96	76.97	10.03	186.21
	20	70.82	76.58	8.13	238.86
200	5	64.98	77.39	18.96	84.21
	10	68.02	76.93	13.10	148.49
	15	70.37	76.62	8.88	235.72
	20	70.95	76.51	7.84	325.39
250	5	65.35	77.12	18.01	97.65
	10	68.63	76.75	11.83	171.26
	15	70.92	76.58	7.98	272.74
	20	71.43	76.21	6.96	403.64

improved from $-\infty$ to 71.43 (final value of standard SDDP lower bound) in the first 60 iterations, and increased to only 73.98 in the next 440 iterations. This slow convergence may be attributed to weak Bender's cuts that are generated in the backward pass. Such weak cuts often lead to relaxations of the stage t problems that are not tight – a common trend in Bender's decomposition-based algorithms [48]. The numerical results indicate that DCS alone may not significantly improve computation time and the quality of solutions obtained by the SDDP algorithm.

TABLE III
RESULTS USING THE SDDP+DCS ALGORITHM.

S	$\lvert\Omega_t\rvert$	z_ℓ	z_u	Gap %	Time (mins)
50	5	64.03	78.05	21.89	33.67
	10	68.25	77.61	13.71	49.29
	15	70.04	77.18	10.19	66.27
	20	71.26	77.01	8.08	87.25
100	5	65.57	77.93	18.85	48.58
	10	69.72	77.34	10.93	73.46
	15	71.23	77.16	8.30	101.28
	20	72.61	76.92	5.97	148.65
150	5	67.03	77.39	15.46	60.09
	10	70.04	77.19	10.04	102.25
	15	72.27	76.89	6.43	156.43
	20	73.06	76.45	4.61	195.23
200	5	68.17	77.41	13.55	73.21
	10	70.92	76.90	8.43	112.28
	15	72.89	76.69	5.21	179.38
	20	73.21	76.42	4.45	235.29
250	5	68.87	77.41	11.83	86.46
	10	71.11	76.98	7.68	147.76
	15	73.57	76.81	3.96	202.41
	20	73.98	76.15	3.00	311.37

To improve the convergence rate of the lower bounds, and further reduce the computation time, valid inequalities of the form (22) were added to each stage t problem in the backward pass (see Section IV-B). Table IV summarizes the results for the SDDP+DCS+J procedure. The table reveals a dramatic improvement in solution quality as well as computation time. For instance, when $S = 250$ and $|\Omega_t| = 20$, SDDP+DCS+J reduces the gap percentage by factors of 21.75 and 9.36, respectively, as compared to standard SDDP (from 6.96% to 0.32%) and SDDP+DCS (from 3% to 0.32%). These results are highly significant in that a realistic scenario tree with 25 stages yields very high quality solutions (gap of 0.32%) within a reasonable amount of time (206.73 minutes). Figures 4 and 5 illustrate the gap and computation time reductions achieved by using SDDP+DCS+J for different values of $|\Omega_t|$.

TABLE IV
RESULTS USING THE SDDP+DCS+J ALGORITHM.

S	$\lvert\Omega_t\rvert$	z_ℓ	z_u	Gap %	Time (mins)
50	5	70.12	77.98	11.21	16.65
	10	72.93	77.46	6.24	24.28
	15	74.17	77.19	4.07	36.69
	20	75.03	76.97	2.23	49.63
100	5	71.47	77.81	8.87	25.97
	10	73.54	77.34	5.13	37.80
	15	74.97	77.15	2.91	54.32
	20	75.45	76.82	1.84	71.21
150	5	72.12	77.72	7.77	38.57
	10	74.32	77.29	4.56	68.43
	15	75.59	76.83	1.64	101.36
	20	75.67	76.29	0.89	150.26
200	5	72.96	77.43	6.13	50.45
	10	75.01	77.16	2.95	83.53
	15	75.71	76.86	1.52	121.62
	20	75.98	76.28	0.45	179.97
250	5	73.21	77.41	6.03	64.36
	10	75.06	77.01	2.83	98.14
	15	75.89	76.85	1.34	141.42
	20	75.99	76.19	0.32	206.73

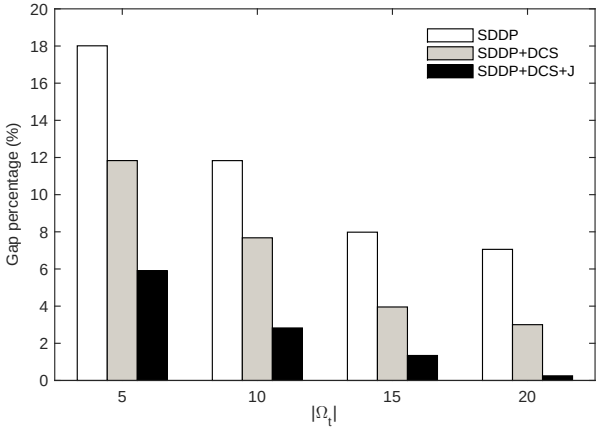

Fig. 4. Gap percentage for different values of $|\Omega_t|$ when $S = 250$.

Moreover, the numerical experiments suggest a significant improvement in the convergence rate of the lower bounds for SDDP+DCS+J, compared to the other two SDDP variants. For example, when $S = 250$ and $|\Omega_t| = 20$, the SDDP+DCS+J lower bound attained the final value of the SDDP+DCS lower bound ($z_\ell = 73.98$) in only 20 iterations. Furthermore, the lower bounds increased by only 5×10^{-4} in the final 300 iterations of SDDP+DCS+J, indicating convergence of the lower bounds. It is noteworthy that a mere 2.7% improvement (73.98 to 75.99) in the lower bound of SDDP+DCS+J, over that of the SDDP+DCS, caused the gap percentage to drop by nearly 2.7% (3% to 0.32%). The comparisons are even more stark between the standard SDDP and SDDP+DCS+J. A mere

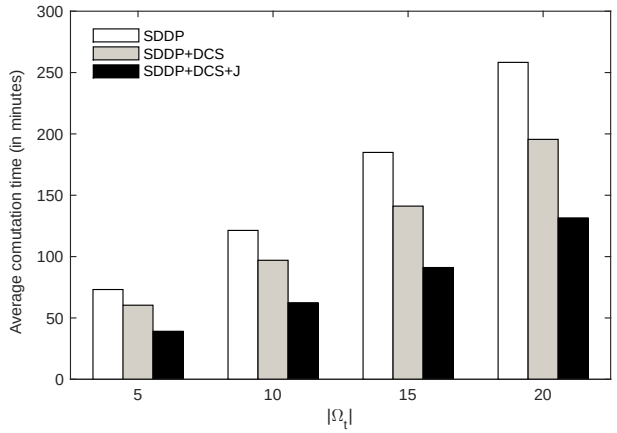

Fig. 5. Average computation time for different values of $|\Omega_t|$.

6.38% (71.43 to 75.99) increase in z_ℓ reduced the gap from 6.96% to 0.32%.

Figure 6 depicts box plots of the lower bounds obtained for the SDDP, SDDP+DCS, and SDDP+DCS+J algorithms. It is noted that the lower bounds obtained by SDDP+DCS+J are not only stronger, but also less variable, as compared to the those of standard SDDP and SDDP+DCS. This is because the Jensen's inequality-based Bender's cuts lead to stronger relaxations and, therefore, tighter lower bounds. That is, as the number of iterations increases, the relaxations become progressively stronger as a large number of high-quality Bender's cuts are added. Furthermore, the computation time decreases because DCS retains only the strong, active cuts from prior iterations. Consequently, the lower bounds converge rapidly, and the computation time decreases significantly using SDDP+DCS+J. By contrast, the variability of lower bounds obtained by standard SDDP and SDDP+DCS are of the same order because the DCS heuristic does not generate stronger cuts; it simply reduces the number of cuts that are retained from prior iterations during the current iteration. Figure 6 confirms our conjecture that SDDP+DCS+J generates much tighter lower bounds, and therefore, solutions with small gap percentages.

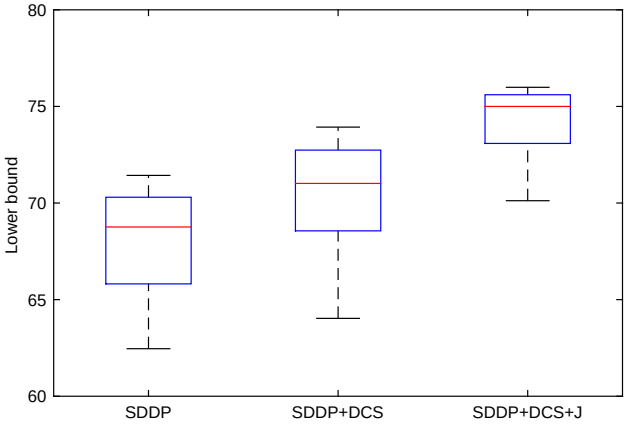

Fig. 6. Box plots of the lower bounds obtained via SDDP and its two variants.

Next, we compared the approximate solutions of SDDP+DCS+J to solutions obtained using a myopic, price-based threshold (MPT) policy that ignores the future impact of current storage and power-flow decisions. The MPT policy maximizes the charging or discharging quantities at each stage, subject to the feasibility constraints (3)–(13), depending on whether the price realized at that stage is below or above a fixed price threshold, respectively. That is, for a given scenario $\omega \in \Omega$, the MPT policy, denoted by $x^\phi(\omega) \equiv (x_t^\phi(\omega))_{t\in T'}$, was obtained by solving a sequence of stage t problems

$$x_t^\phi(\omega) = \operatorname{argmax} \sum_{i\in C'} m_t^i \mathbb{I}_{[p_t<\bar{p}]} + n_t^i \mathbb{I}_{[p_t\geq\bar{p}]}$$
$$\text{s.t.} \quad F_t x_t = h_t(\omega_t) - G_t x_{t-1}^\phi(\omega),$$

where $x_{t-1}^\phi(\omega)$ is the MPT decision vector at stage $t-1$, $\bar{p}$ is a known price threshold and $\mathbb{I}_A$ denotes the indicator function of event A. In these experiments, the threshold $\bar{p}$ was set to the sample mean of the prices in the PJM pricing data. Specifically,

$$\bar{p} = \frac{1}{24}\sum_{t=2}^{25} \bar{p}_t \approx \$35.79/\text{MWh}.$$

The one-step cost at stage t using the MPT policy is denoted by $c_t' x_t^\phi(\omega)$ and is calculated via (14). Then, the total cost over the horizon for scenario ω is

$$z_\phi(\omega) = c_1' x_1^\phi + \sum_{t\in T'} c_t' x_t^\phi(\omega).$$

Let z_ϕ denote the average MPT policy cost of S distinct forward-pass scenarios used in SDDP+DCS+J.

The expected cumulative costs incurred over the planning horizon were compared using SDDP+DCS+J, the MPT policy, and the corresponding model when no energy storage is available (for the case $S = 250$ and $|\Omega_t| = 20$). The expected cumulative cost at hour t is the sum of accumulated costs up to that hour, so the expected cost at hour 24 is the expected total cost incurred over the planning horizon. In the absence of storage capacity, we set $x_1 = 0$; therefore, there are no charging or discharging decisions in each of the subsequent stages. Denote the cost of the no-storage policy by z_N. Figure 7 reveals that the SDDP+DCS+J policy significantly reduces cumulative costs in each stage. Specifically, the total horizon costs are reduced by 25.65% (from 102.47 to 76.19) as compared to the MPT policy, and by 48.68% (from 143.67 to 76.19) as compared to the policy that does not use energy storage.

Figure 8 depicts the average battery levels for the SDDP+DCS+J and MPT policies and the average electricity price in each hour of the day. The battery can be charged up to its maximum SOC level ($\gamma_{\max} x_1$) at the start of the planning horizon. The data revealed that hours 1 to 10, on average, had low price and high wind-generation levels. Therefore, the battery retains most of its initial charge during hours 1 to 10 under the SDDP+DCS+J policy. The MPT policy does not discharge energy (on average) during hours 1 to 10 because the prices (on average) are less than the price threshold $\bar{p}$ in these periods. As prices increase and wind generation decreases in subsequent periods, energy is discharged from

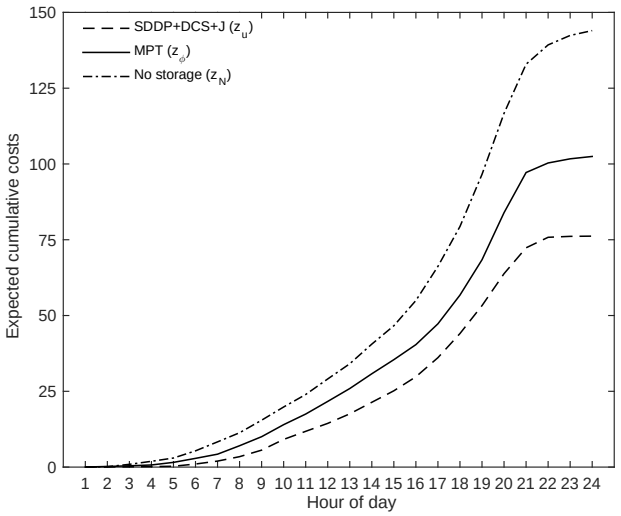

Fig. 7. Expected cumulative costs over the planning horizon.

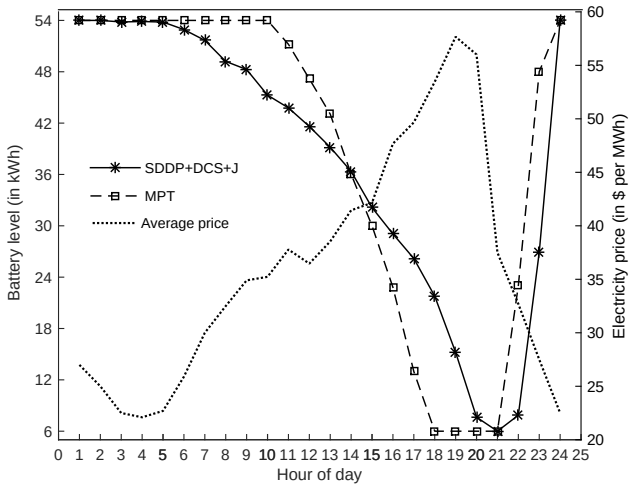

Fig. 8. Average battery level and average price for each hour.

the battery to satisfy the demand under both of these policies. Not surprisingly, the battery is discharged to its minimum SOC level ($\gamma_{\min} x_1$) during the peak-price periods (hours 18 to 21) in both cases.

Although the initiation of discharging is earlier in SDDP+DCS+J (hour 6) compared to the MPT policy (hour 11), the MPT battery levels fall dramatically once discharge is initiated in hour 11. This is because the MPT policy maximizes the energy discharged from the battery between hours 11 to 21, when prices, on average, are greater than the threshold level $\bar{p}$. It is noted that for the MPT policy, the battery level reaches the minimum SOC level as early as hour 18, thereby forcing procurement of electricity during hours 18 to 21 when the (average) prices are highest. This behavior is reflected in Figure 7 by the steep slope of the cumulative-cost curve of the MPT policy between hours 18 to 21. Thus, the MPT policy effectively diminishes the advantage of using stored energy – namely to reduce peak-period costs. By contrast, the policy obtained via SDDP+DCS+J is intelligent in that it prescribes the use of stored energy during peak-price periods, thereby reducing the overall expected costs over the horizon. Figure 8 highlights the benefits of time-shifting energy consumption via storage in a microgrid. Although the two policies exhibit similar behavior over time, the SDDP+DCS+J policy accounts for the future impact of current decisions, yielding better operational decisions that lead to significant cost savings.

Next, we compared the solutions of the multistage SP model to those obtained by solving an associated two-stage SP model in which the non-anticipativity condition is relaxed. The two-stage model allows for only a single recourse opportunity in stage 2. The stage 2 recourse decisions for a realized scenario $\omega \in \Omega$ are collected in the vector $x(\omega) \equiv (x_t(\omega) : t \in T')$. For notational convenience, we drop the dependence of x on ω and simply write x. Let $c \equiv (c_t : t \in T')$ be the corresponding second-stage cost vector (also a function of ω). The stage 1 problem is

$$\check{z} = \min_{x_1} \; c_1' x_1 + \mathbb{E}[Q(x_1, \omega)] \tag{27a}$$

$$\text{s.t.} \;\; 0 \leq \sum_{i \in C'} x_1^i \leq \alpha, \tag{27b}$$

and the stage 2 problem is

$$Q(x_1, \omega) = \min_{x} \; c' x \tag{28a}$$

$$\text{s.t.} \;\; Fx = h(\omega) - G x_1. \tag{28b}$$

The matrices F and G and vector $h(\omega)$ were obtained by reformulating constraints (3) – (13) together for all stages $t \in T'$. The SDDP+DCS+J algorithm was used to solve model (27) approximately. The lower and upper bounds of the optimal value $\check{z}$ are denoted by $\check{z}_\ell$ and $\check{z}_u$, respectively. Table V summarizes the results of the two-stage SP model.

TABLE V
TWO-STAGE RESULTS USING THE SDDP+DCS+J ALGORITHM.

S	$\lvert\Omega\rvert$	$\check{z}_\ell$	$\check{z}_u$	Gap %	Time (mins)
50	10^4	80.02	82.86	3.55	7.57
	3×10^4	80.93	82.54	1.99	20.26
100	10^4	80.21	82.69	3.09	15.48
	3×10^4	81.61	82.43	1.00	46.23
150	10^4	80.52	82.48	2.45	24.86
	3×10^4	81.88	82.37	0.59	73.39
200	10^4	80.73	82.38	2.04	37.12
	3×10^4	81.96	82.37	0.50	101.72
250	10^4	81.01	82.36	1.67	56.75
	3×10^4	82.13	82.36	0.28	148.27

Similar to the results of the multistage model, the gap percentage for the two-stage model decreases as both S and $|\Omega|$ increase, while the computation time increases. Of far greater interest, however, is the comparison between the solution bounds of the multistage and two-stage models. Let $\check{z}_u^*$ and z_u^* denote the best upper bound obtained for the two-stage and multistage models, respectively, for a particular number of forward-pass scenarios S. We compared these upper bounds

for each $S \in \{50, 100, 150, 200, 250\}$ using

$$\Delta_S(\%) = \frac{\check{z}_u^* - z_u^*}{\check{z}_u^*} \times 100,$$

where Δ_S denotes the cost savings over the planning horizon (as a percentage) when multiple recourse opportunities are available. Table VI provides strong evidence that substantial cost savings are achieved by using the multistage SP model.

TABLE VI
TWO-STAGE VERSUS MULTISTAGE SP UPPER BOUNDS.

S	$\check{z}_u^*$	z_u^*	$\Delta_S(\%)$
100	82.54	76.97	6.75
200	82.43	76.82	6.81
300	82.37	76.29	7.38
400	82.37	76.28	7.39
500	82.36	76.19	7.49

Finally, to examine scalability issues associated with our solution procedure, we solved a simplified two-bus system and compared its results with the 4-bus system. As depicted in Figure 9, the two-bus system is configured by aggregating the loads of the 4-bus system into a single bus that is connected to the wind turbine and a single storage device.

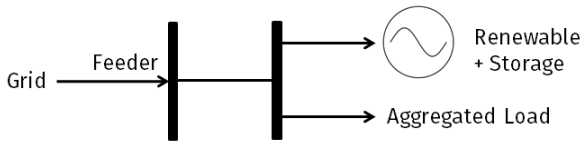

Fig. 9. A two-bus, grid-connected microgrid.

The aggregated net demand components in the two-bus system are assumed to follow truncated normal distributions

$$\tilde{r}_t \sim TN(\bar{r}_t, \hat{r}_t), \quad t \in T',$$
$$\tilde{w}_t \sim TN(\bar{w}_t, \hat{w}_t), \quad t \in T',$$

where the corresponding means and variances are as follows:

$$\bar{r}_t = \sum_{i \in C'} \bar{r}_t^i; \quad \hat{r}_t = \sum_{i \in C'} \hat{r}_t^i;$$
$$\bar{w}_t = \sum_{i \in C'} \bar{w}_t^i; \quad \hat{w}_t = \sum_{i \in C'} \hat{w}_t^i.$$

The price distributions are identical to those of the 4-bus system, and the two-bus system has a single line constraint. The model parameters for the two-bus system were set to the values given in Table I. The model was solved using the SDDP+DCS+J procedure. Table VII summarizes the results for the case $S = 250$, as it provides the best gap percentages.

It is noted that gaps below 1% were obtained for all values of $|\Omega_t| \geq 10$. Moreover, the computation times are strikingly smaller. For example, a 25-stage scenario-tree with $|\Omega_t| = 20$ was solved in less than 1.5 hours with a gap of only 0.18%. Figure 10 compares the computation time between the two systems for different values of $|\Omega_t|$. The results are intuitive due to dimensionality reduction of the two-bus system. However, it is interesting to note that the computation time does not appear to scale exponentially with problem size. This provides affirmative evidence of the scalability of the SDDP+DCS+J algorithm to problems with multiple scales.

TABLE VII
RESULTS USING SDDP+DCS+J FOR THE TWO-BUS MICROGRID.

$\lvert\Omega_t\rvert$	z_ℓ	z_u	Gap %	Time (mins)
5	54.62	56.15	2.90	17.36
10	55.06	55.54	0.87	35.32
15	55.32	55.52	0.36	58.54
20	55.41	55.51	0.18	84.75

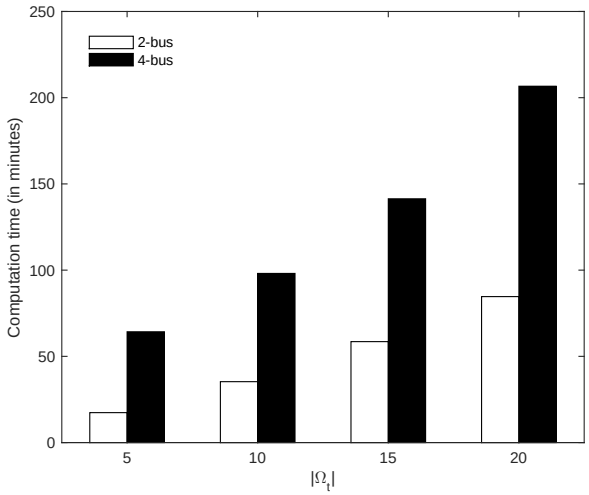

Fig. 10. Computation time for different values of $|\Omega_t|$ when $S = 250$.

VI. CONCLUSION

In this paper, we have presented a multistage stochastic programming model to obtain viable energy procurement and storage strategies for grid-connected microgrids. The model includes three sources of uncertainty: demand, renewable generation, and real-time electricity prices. This framework enables microgrid operators to determine the appropriate amount of electricity to procure from the main grid and the amount to charge to, or discharge from, local storage devices, to satisfy demand and power flow requirements during each stage of a finite planning horizon. Our extensive computational study on a realistic 4-bus microgrid revealed that the multistage stochastic programming model achieves significant cost reductions as compared to myopic and non-storage policies, as well as policies obtained using a two-stage SP formulation. Moreover, our customized SDDP algorithm is able to address the computational challenges associated with the multistage structure of the problem. Our customization, which uses dynamic cut selection and a novel lower bound improvement strategy, drastically outperforms the standard SDDP algorithm and also demonstrates its scalability to potentially much larger problem instances. It is also conjectured that our improved solution method can be extended to address the computational issues of multistage electric generation expansion and hydropower scheduling problems.

While the multistage stochastic programming model is very useful for prescribing solutions that reduce total electricity costs, it can be improved in several important ways. First, it will be instructive to model the case in which the microgrid operators have the flexibility to sell excess power back to the main grid and exploit arbitrage opportunities in electricity markets. This feature is likely to alter the microgrid's procurement and storage strategies significantly. Second, the stage-wise independence assumption of the uncertain variables may be restrictive. For example, price and wind generation levels may exhibit autocorrelation over time; therefore, it will be instructive in future work to explore solution approaches that relax the stage-wise independence assumption. Third, more sophisticated sampling procedures, such as importance sampling, and other variance reduction techniques, can be used to identify a set of scenarios that balances the exploration-exploitation tradeoff in the SDDP algorithm (see [54] for additional details). Finally, extending the the SDDP algorithms to handle problems of higher dimensionality is an important area of future work.

ACKNOWLEDGMENT

We are grateful to five anonymous referees, and the Associate Editor, for their constructive comments. This research was supported, in part, by grants from the Mascaro Center for Sustainable Innovation and the Center for Industry Studies (CIS) at the University of Pittsburgh.

REFERENCES

[1] N. Hatziargyriou, H. Asano, R. Iravani, and C. Marnay, "Microgrids," *IEEE Power and Energy Magazine*, vol. 5, no. 4, pp. 78–94, 2007.

[2] A. Khodaei, S. Bahramirad, and M. Shahidehpour, "Microgrid planning under uncertainty," *IEEE Transactions on Power Systems*, vol. 30, no. 5, pp. 2417–2425, 2015.

[3] Y. Zhang, N. Gatsis, and G. B. Giannakis, "Robust energy management for microgrids with high-penetration renewables," *IEEE Transactions on Sustainable Energy*, vol. 4, no. 4, pp. 944–953, 2013.

[4] B. Roberts and C. Sandberg, "The role of energy storage in development of smart grids," *Proceedings of the IEEE*, vol. 99, no. 6, pp. 1139–1144, 2011.

[5] S. Suryanarayanan, F. David, J. Mitra, and Y. Li, "Achieving the smart grid through customer-driven microgrids supported by energy storage," in *Proceedings of the IEEE International Conference on Industrial Technology (ICIT)*, 2010, pp. 884–890.

[6] J. Kaldellis and D. Zafirakis, "Optimum energy storage techniques for the improvement of renewable energy sources-based electricity generation and economic efficiency," *Energy*, vol. 32, no. 12, pp. 2295–2305, 2007.

[7] I. Atzeni, L. G. Ordóñez, G. Scutari, D. P. Palomar, and J. R. Fonollosa, "Day-ahead bidding strategies for demand-side expected cost minimization," in *IEEE International Conference on Smart Grid Communications (SmartGridComm)*, 2012, pp. 91–96.

[8] C. Gouveia, J. Moreira, C. L. Moreira, and J. A. P. Lopes, "Coordinating storage and demand response for microgrid emergency operation," *IEEE Transactions on Smart Grid*, vol. 4, no. 4, pp. 1898–1908, 2013.

[9] M. Lijesen, "The real-time price elasticity of electricity," *Energy Economics*, vol. 29, no. 2, pp. 249–258, 2007.

[10] B. Dunn, H. Kamath, and J. Tarascon, "Electrical energy storage for the grid: A battery of choices," *Science*, vol. 334, no. 6058, pp. 928–935, 2011.

[11] Z. Wang and M. Lemmon, "Stability analysis of weak rural electrification microgrids with droop-controlled rotational and electronic distributed generators," in *Proceedings of the IEEE Power Energy Society General Meeting*, 2015, pp. 1–5.

[12] K. Ahlert and C. van Dinther, "Sensitivity analysis of the economic benefits from electricity storage at the end consumer level," in *Proceedings of the IEEE PowerTech Conference*, 2009, pp. 1–8.

[13] W. Hu, Z. Chen, and B. Bak-Jensen, "Optimal operation strategy of battery energy storage system to real-time electricity price in Denmark," in *Proceedings of the IEEE Power and Energy Society General Meeting*, 2010, pp. 1–7.

[14] P. Van de Ven, N. Hegde, L. Massoulie, and T. Salondis, "Optimal control of end-user energy storage," *IEEE Transactions on Smart Grid*, vol. 4, no. 2, pp. 789–797, 2013.

[15] C. Hill, M. Such, D. Chen, J. Gonzalez, and W. Grady, "Battery energy storage for enabling integration of distributed solar power generation," *IEEE Transactions on Smart Grid*, vol. 3, no. 2, pp. 850–857, 2012.

[16] I. Koutsopoulos, V. Hatzi, and L. Tassiulas, "Optimal energy storage control policies for the smart power grid," in *IEEE International Conference on Smart Grid Communications*, 2011, pp. 475–480.

[17] J. Birge and F. Louveaux, *Introduction to Stochastic Programming, Second Edition*. New York, NY: Springer, 2011.

[18] D. Lee, J. Kim, and R. Baldick, "Stochastic optimal control of the storage system to limit ramp rates of wind power output," *IEEE Transactions on Smart Grid*, vol. 4, no. 4, pp. 2256–2265, 2013.

[19] Y. Ji, J. Wang, S. Yan, W. Gao, and H. Li, "Optimal microgrid energy management integrating intermittent renewable energy and stochastic load," in *IEEE Advanced Information Technology, Electronic and Automation Control Conference (IAEAC)*, 2015, pp. 334–338.

[20] X. Xi, R. Sioshansi, and V. Marano, "A stochastic dynamic programming model for co-optimization of distributed energy storage," *Energy Systems*, vol. 5, no. 3, pp. 475–505, 2014.

[21] J. García-González, R. de la Muela, L. Santos, and A. González, "Stochastic joint optimization of wind generation and pumped-storage units in an electricity market," *IEEE Transactions on Power Systems*, vol. 23, no. 2, pp. 460–468, 2008.

[22] S. Talari, M. Yazdaninejad, and M. Haghifam, "Stochastic-based scheduling of the microgrid operation including wind turbines, photovoltaic cells, energy storages and responsive loads," *IET Generation, Transmission Distribution*, vol. 9, no. 12, pp. 1498–1509, 2015.

[23] Z. Zhou, J. Zhang, P. Liu, Z. Li, M. C. Georgiadis, and E. N. Pistikopoulos, "A two-stage stochastic programming model for the optimal design of distributed energy systems," *Applied Energy*, vol. 103, pp. 135–144, 2013.

[24] B. Moradzadeh and K. Tomsovic, "Two-stage residential energy management considering network operational constraints," *IEEE Transactions on Smart Grid*, vol. 4, no. 4, pp. 2339–2346, 2013.

[25] S. Ahmed, "Two-stage stochastic integer programming: A brief introduction," in *Wiley Encyclopedia of Operations Research and Management Science*, J. Cochran, L. Cox, P. Keskinocak, J. Kharoufeh, and J. Smith, Eds. John Wiley & Sons, Inc., 2011.

[26] J. Birge, "Decomposition and partitioning methods for multistage stochastic linear programss," *Operations Research*, vol. 33, no. 5, pp. 989–1007, 1985.

[27] A. Shapiro, "Analysis of stochastic dual dynamic programming method," *European Journal of Operational Research*, vol. 209, no. 1, pp. 63–72, 2011.

[28] V. de Matos, A. Philpott, and E. Finardi, "Improving the performance of Stochastic Dual Dynamic Programming," *Journal of Computational and Applied Mathematics*, vol. 290, pp. 196–208, 2015.

[29] W. Yuan, J. Wang, F. Qiu, C. Chen, C. Kang, and B. Zeng, "Robust optimization-based resilient distribution network planning against natural disasters," *IEEE Transactions on Smart Grid*, vol. 7, no. 6, pp. 2817–2826, 2016.

[30] W. Shi, X. Xie, C. Chu, and R. Gadh, "Distributed optimal energy management in microgrids," *IEEE Transactions on Smart Grid*, vol. 6, no. 3, pp. 1137–1146, 2015.

[31] O. Ardakanian, S. Keshav, and C. Rosenberg, *Integration of renewable generation and elastic loads into distribution grids*. Springer International, 2016.

[32] Y. Ghiassi-Farrokhfal, F. Kazhamiaka, C. Rosenberg, and S. Keshav, "Optimal design of solar PV farms with storage," *IEEE Transactions on Sustainable Energy*, vol. 6, no. 4, pp. 1586–1593, 2015.

[33] H. Yeh and S. Doan, "Battery placement on performance of VAR controls," in *IEEE Green Energy and Systems Conference*, 2013, pp. 1–6.

[34] P. Van de Ven, N. Hegde, L. Massoulie, and T. Salondis, "Optimal control of residential energy storage under price fluctuations," in *Proceedings of the First International Conference on Smart Grids, Green Communications and IT Energy-Aware Technologies*, 2011, pp. 159–162.

[35] P. Yang and A. Nehorai, "Joint optimization of hybrid energy storage and generation capacity with renewable energy," *IEEE Transactions on Smart Grid*, vol. 5, no. 4, pp. 1566–1574, 2014.

[36] S. Bahramirad, W. Reder, and A. Khodaei, "Reliability-constrained optimal sizing of energy storage system in a microgrid," *IEEE Transactions on Smart Grid*, vol. 3, no. 4, pp. 2056–2062, 2012.
[37] Y. Huang, W. Hu, Y. Min, W. Zhang, W. Luo, Z. Wang, and W. Ge, "Risk-constrained coordinative dispatching for battery energy storage systems of wind farms," in *IEEE PES Asia-Pacific Power and Energy Engineering Conference (APPEEC)*, 2013, pp. 1–6.
[38] C. Chen, J. Wang, F. Qiu, and D. Zhao, "Resilient distribution system by microgrids formation after natural disasters," *IEEE Transactions on Smart Grid*, vol. 7, no. 2, pp. 958–966, 2016.
[39] S. Tan, J. Xu, and S. Panda, "Optimization of distribution network incorporating distributed generators: An integrated approach," *IEEE Transactions on Power Systems*, vol. 28, no. 3, pp. 2421–2432, 2013.
[40] Z. Wang, B. Chen, J. Wang, J. Kim, and M. Begovic, "Robust optimization based optimal dg placement in microgrids," *IEEE Transactions on Smart Grid*, vol. 5, no. 5, pp. 2173–2182, 2014.
[41] R. Walling, R. Saint, R. Dugan, J. Burke, and L. Kojovic, "Summary of distributed resources impact on power delivery systems," *IEEE Transactions on Power Delivery*, vol. 23, no. 3, pp. 1636–1644, 2008.
[42] W. E. Featheringill, "Power transformer loading," *IEEE Transactions on Industry Applications*, vol. IA-19, no. 1, pp. 21–27, 1983.
[43] P. Sŭlc, S. Backhaus, and M. Chertkov, "Optimal distributed control of reactive power via the alternating direction method of multipliers," *IEEE Transactions on Energy Conversion*, vol. 29, no. 4, pp. 968–977, 2014.
[44] Q. Zheng, J. Wang, and A. Liu, "Stochastic optimization for unit commitment – A review," *IEEE Transactions on Power Systems*, vol. 30, no. 4, pp. 1913–1924, 2015.
[45] L. Kuznia, B. Zeng, G. Centeno, and Z. Miao, "Stochastic optimization for power system configuration with renewable energy in remote areas," *Annals of Operations Research*, vol. 210, no. 1, pp. 411–432, 2013.
[46] A. Shapiro, W. Tekaya, J. da Costa, and M. Soares, "Risk neutral and risk averse stochastic dual dynamic programming method," *European Journal of Operational Research*, vol. 224, no. 2, pp. 375–391, 2013.
[47] M. Pereira and L. Pinto, "Multi-stage stochastic optimization applied to energy planning," *Mathematical Programming*, vol. 52, no. 1, pp. 359–375, 1991.
[48] L. Tang, W. Jiang, and G. Saharidis, "An improved Benders decomposition algorithm for the logistics facility location problem with capacity expansions," *Annals of Operations Research*, vol. 210, no. 1, pp. 165–190, 2012.
[49] S. Batun, B. Denton, T. Huschka, and A. Schaefer, "Operating room pooling and parallel surgery processing under uncertainty," *INFORMS Journal on Computing*, vol. 23, no. 2, pp. 220–237, 2011.
[50] S. Resnick, *A Probability Path*. Boston, MA: Birkhäuser, 2005.
[51] A. Celik, "Energy output estimation for small-scale wind power generators using weibull-representative wind data," *Journal of Wind Engineering and Industrial Aerodynamics*, vol. 91, no. 5, pp. 693–707, 2003.
[52] A. Cutis and V. Gevorgian, "Wind turbine generator system power quality test report for the Gaia wind 11-kW wind turbine," National Renewable Energy Laboratory, Tech. Rep., 2011.
[53] M. Lee, G. C. Shaw, and V. Modi, "Battery storage: Comparing shared to individually owned storage given rural demand profiles of a cluster of customers," in *IEEE Global Humanitarian Technology Conference (GHTC)*, 2014, pp. 200–206.
[54] V. Kozmik, "On variance reduction of mean-CVar Monte Carlo estimators," *Computational Management Science*, vol. 12, no. 2, pp. 221–242, 2014.
[55] L. Pan and D. Politis, "Bootstrap prediction intervals for linear, nonlinear and nonparametric autoregressions," *Journal of Statistical Planning and Inference*, vol. 42, no. 1, pp. 27–62, 2014.